On the reduction of natural convection heat transfer in horizontal eccentric annuli containing saturated porous media

Received October 1995
Revised August 1996

J.P. Barbosa Mota
IBET – Instituto de Biologia Experimental e Tecnológica, Oeiras, Portugal, and
E. Saatdjian
Laboratoire d'Energétique et de Méchanique Théorique et Appliquée, ENSEM, Vandoeuvre, France

Nomenclature

a = scale factor in bipolar co-ordinates, $\sinh\alpha_i$
e = vertical distance between the cylinders' centres
g = gravitational acceleration
Nu = global Nusselt number
N_α, N_β = number of grid points in the α and β directions
Q = total heat flow in the annular region
r = radius
R = radius ratio
Ra = Rayleigh number
t = dimensionless time
T = dimensionless temperature, $(\hat{T} - \hat{T}_o)/(\hat{T}_i - \hat{T}_o)$
$\hat{T}$ = temperature

Greek symbols

α, β = bipolar coordinates
ε = eccentricity, $e/(r_o - r_i)$
κ = permeability of the medium
λ_{eq} = equivalent thermal conductivity of the medium
ν = kinematic viscosity of the fluid
ξ = thermal expansion coefficient of the fluid
$(\rho c)_f$ = heat capacity of the fluid
ψ = dimensionless stream function

Subscripts

i = inner cylinder
o = outer cylinder
i, j = location in the grid

Introduction

Natural convection in horizontal porous annuli has a wide variety of technological applications such as the insulation of an aircraft cabin or horizontal pipes, cryogenics, the storage of thermal energy, and underground cable systems, to mention just a few. The case considered here, probably of the most practical significance, is one in which the cylinders' surfaces are

Financial support received from JNICT (PBIC/P/QUIT/2415/95) and from Program PRAXIS XXI (BPD/6066/95) is gratefully acknowledged.

International Journal for Numerical Methods for Heat & Fluid Flow
Vol. 7 No. 4, 1997, pp. 401-416.

impermeable and maintained at constant uniform temperatures, with the inner temperature being higher than the outer. As a result of the temperature difference, buoyancy-driven flow is induced in the medium.

The phenomenology of the problem can be pictured as follows. When the temperature difference between the walls of the two cylinders is small, the fluid motion is two-dimensional and consists of two symmetrical counter-rotating cells, one in each half of the annulus. As the temperature difference between the two cylinders increased so does the intensity of the convective phenomena, and the isotherms, which initially were concentric, start to become distorted in the upper part of the annulus. In the region located beneath the hot inner cylinder, the isotherms get closer to the wall creating a stagnant region in which the heat transfer takes place largely by conduction. When the thermal field is sufficiently distorted an instability appears in the upper part of the annulus under the form of either multicellular two-dimensional patterns or three-dimensional time-dependent structures. It is not yet clear which type of instabilities will occur for a given Rayleigh number and geometrical parameters, but the three-dimensional motion will eventually prevail in the layer if the temperature difference in the annulus is increased sufficiently. As long as the flow remains two-dimensional the problem is dependent on two parameters: the radius ratio R and the Darcy-Rayleigh number Ra.

The case of concentric cylinders has received the most attention in the literature. Caltagirone[1] used the Christiansen effect to visualize the isotherms in an annulus of radius ratio $R = 2$, and determined experimental Nusselt numbers based on temperature measurements of the thermal field. At high Rayleigh numbers, the flow was reported to have changed to a three-dimensional oscillatory motion, partially confirmed by a finite element simulation, which led the author to conclude that multicellular two-dimensional structures do not exist. In the same study, the equations governing the two-dimensional convective motion were solved using finite differences, but owing to an insufficient number of grid points Caltagirone was unable to obtain other flow regimes in addition to the bicellular one.

Fukuda *et al.*[2] obtained three-dimensional results using the finite difference method for an inclined annulus. However, the results could not be extended to the horizontal case owing to the presence of the component of the gravitational force in the axial direction of the annulus which is not present in the horizontal case. Later, Rao *et al.*[3,4] studied numerically the horizontal annulus in both two and three dimensions using the Galerkin method. These authors obtained, in addition to the bicellular flow pattern, two other possible two-dimensional multicellular numerical solutions (with four and six cells) depending on the initial conditions.

Recent two-dimensional numerical work by Barbosa Mota and Saatdjian[5-7], using very fine grids, has shown that when R is above 1.75, the transition from a two-cell to a four-cell flow regime depends on whether the Rayleigh number is increased or decreased and a closed hysteresis loop is formed associated with the transition from one flow pattern to the other. For small

radius ratios ($R < 1.75$), steady-state flow regimes containing two, four, six and eight cells are progressively obtained in the porous layer as the Rayleigh number is increased, but no hysteresis behaviour is observed. The study also shows that reducing the radius ratio increases flow stability by shifting the convective effects to higher Rayleigh numbers. The behaviour described above is in agreement with an earlier study of bifurcation phenomena carried out by Himasekhar and Bau[8] using regular perturbation expansion techniques and the Galerkin method. These authors state that for $R > 2^{1/4}$ two solutions remain stable for some range of Ra above the transitional value; for $R < 2^{1/2}$, the additional solutions appear via a simple bifurcation process, i.e. one solution branch loses stability while another one gains it.

In one of the experiments using the Christiansen effect on an annulus of radius ratio $R = 2$, Charrier-Mojtabi *et al.*[9] observed the two-dimensional bicellular flow pattern when the Rayleigh number was increased up to 250, after which three-dimensional effects became visible in the upper part of the annular region. When the Rayleigh number was progressively reduced (cooling phase), the flow pattern became two-dimensional again and consisted of four convective cells which persisted until the Rayleigh number reached the transitional value. This experiment proved the existence of two-dimensional four-cell flow structures and seems to confirm the hysteresis behaviour obtained numerically by Barbosa Mota and Saatdjian[5-7].

The observation that the reduction of the radius ratio defers the convective effects to higher Rayleigh numbers has led to the study of the eccentric geometry, since it may lead to a reduction of the heat losses. The reason is that moving the inner cylinder upwards, so that its centre is above the centre of the outer cylinder, decreases the local thickness of the upper part of the annulus where the convective effects are stronger, therefore reducing the impact of the convective heat transfer. On the other hand, the decrease of the gap spacing in the top part of the layer increases the conductive heat losses. For each pair of values (R, Ra) there is an optimum value of the eccentricity for which the overall heat transfer is a minimum.

The eccentric annulus was studied numerically by Bau *et al.* using both finite differences[10] and regular perturbation expansion techniques. Using a two-term regular perturbation expansion Bau[11] investigated three different geometrical configurations: an eccentric annulus, a buried pipe, and two cylinders, one outside the other. An extension[12] of the perturbation expansion for the case of an eccentric annulus, enabled the Nusselt number to be expressed as a power series of Ra up to $O(Ra^{30})$. Although the results presented apply for small Rayleigh numbers only, it is concluded in both studies that the heat losses can be reduced with respect to the concentric case. In a later study, Himasekhar and Bau[13] used a boundary-layer technique to obtain a correlation for the Nusselt number as a function of Ra and the geometrical parameters, valid for a larger range of Rayleigh numbers.

In the works discussed above, the study of the reduction of the heat losses by the use of eccentric insulations has been restricted to one flow pattern, the

two-dimensional bicellular one, which is clearly not the only flow pattern that can occur in reality. In the parameter ranges (R, Ra) employed in those studies, both multicellular and three-dimensional flows are physically realizable; these have higher heat transfer rates than does the bicellular flow, therefore affecting the optimum value of the eccentricity for a given radius ratio and Rayleigh number.

In the present work, the accurate finite-difference code used by Barbosa Mota and Saatdjian[5-7] for two-dimensional convective motion between concentric cylinders is modified in order to investigate the conditions leading to a heat transfer reduction by the use of eccentric annuli. Although two-dimensional studies reduce the generality of the problem, they are computationally attractive and useful from the engineering point of view. Both Barbosa Mota and Saatdjian[6, Figure 6] and Rao *et al.*[3, Figure 10] compared the overall heat transfer rates predicted numerically with experimental data covering both two- and three-dimensional flows, and showed that two-dimensional simulations give a good description of the overall heat transfer in the annulus for a range of Rayleigh numbers that, although limited, extends past the maximum value of Ra under which the two-dimensional bicellular flow is the unique flow pattern.

Mathematical model

The system under study consists of a horizontal eccentric annulus, of inner and outer radii r_i and r_o, containing a saturated porous medium (Figure 1a). The cylinders' surfaces are impermeable and maintained at constant uniform temperatures $\hat{T}_i$ and $\hat{T}_o$, respectively. We focus on two-dimensional phenomena which are symmetrical about the vertical centre line by considering only inner cylinder displacement in the vertical direction.

We formulate the problem in the usual bipolar orthogonal co-ordinates (α, β), also used by Bau[11,12], which are defined by the following transformation:

$$x = \frac{-a \sinh\alpha}{\cosh\alpha - \cos\beta}, \quad y = \frac{a \sin\beta}{\cosh\alpha - \cos\beta}.$$

An example of a bipolar co-ordinate mesh is shown in Figure 1b. There are other orthogonal or non-orthogonal co-ordinate systems that can be used to describe the annular region between two eccentric cylinders. For example, in the study of lubrication in a journal bearing, both Wood[14] and DiPrima and Stuart[15] employed a modified orthogonal bipolar co-ordinate system that becomes identical to cylindrical-polar co-ordinates in the limit of concentric cylinders, whereas Wannier[16] employed a non-orthogonal mixed Cartesian-polar co-ordinate system. The bipolar coordinate system has the advantage of mapping the cylinders' walls to constant α values, α_i and α_o. Strictly speaking, this co-ordinate system does not provide for concentric cylinders. In practice this limitation is not a serious one, since the eccentricity can be decreased as much as one desires.

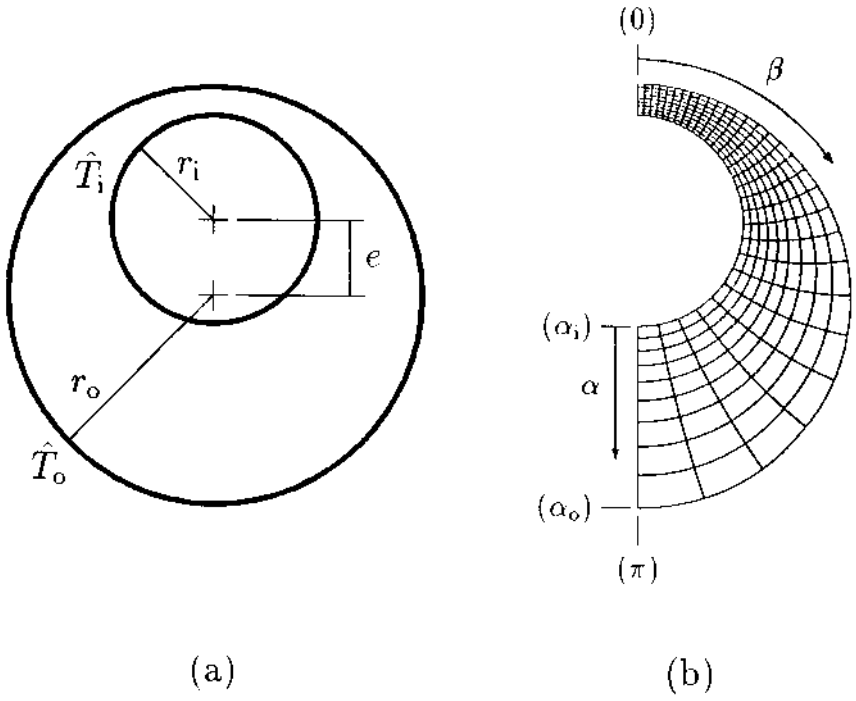

Figure 1. (a) geometrical configuration of the problem; (b) bipolar sample grid for $R = 2$ and $\varepsilon = 0.7$

The fluid motion is assumed to be adequately described by the two-dimensional Darcy-Boussinesq equations, which for the case of inner cylinder vertical displacement only, are expressed in dimensionless form as:

$$h^2 \frac{\partial T}{\partial t} = \nabla^2 T - \frac{\partial \psi}{\partial \alpha}\frac{\partial T}{\partial \beta} + \frac{\partial \psi}{\partial \beta}\frac{\partial T}{\partial \alpha}, \tag{1}$$

$$\nabla^2 \psi = \pm a\, h^2 Ra \left[\sinh \alpha \sin \beta \frac{\partial T}{\partial \alpha} + (1 - \cosh \alpha \cos \beta)\frac{\partial T}{\partial \beta}\right],$$

$$\nabla^2 = \frac{\partial^2}{\partial \alpha^2} + \frac{\partial^2}{\partial \beta^2}, \quad h = \frac{1}{\cosh \alpha - \cos \beta}. \tag{2}$$

In the above equations, ψ is the stream function, T is the temperature, and

$$Ra = \frac{\kappa(\rho c)_f \xi r_i g(\hat{T}_i - \hat{T}_o)}{\nu \lambda_{eq}}$$

is the Darcy-Rayleigh number. In principle, the centre of the inner cylinder can be displaced vertically in both directions so that it can lie above ($e > 0$) or below ($e < 0$) the centre of the outer cylinder. For the first case, i.e. positive eccentricity, the (+) sign is valid in the r.h.s. of (2). Similarly, the (–) sign holds for inner cylinder displacement in the downwards direction.

The boundary conditions on the inner and outer cylinders are, respectively, $\psi = 0$, $T = 1$ for $\alpha = \alpha_i$ and $\psi = 0$, $T = 0$ for $\alpha = \alpha_o$, and the symmetry conditions with respect to the vertical axis are

$$\frac{\partial T}{\partial \beta} = 0, \ \psi = 0 \quad \text{for} \quad \beta = 0, \pi.$$

The values of α_i and α_o are related to the radius ratio R and to the eccentricity ε by

$$R = \frac{r_o}{r_i} = \frac{\sinh \alpha_i}{\sinh \alpha_o} \quad \text{and} \quad \epsilon = \frac{\epsilon}{r_o - r_i} = \frac{\sinh(\alpha_i - \alpha_o)}{\sinh \alpha_i - \sinh \alpha_o}.$$

At steady-state, the total heat flow in the annular region is

$$Q = 2 \int_0^{\pi} \left(\frac{\partial T}{\partial \alpha} \right) \mathrm{d}\beta \quad \text{at} \quad \alpha = \alpha_i \ \text{or} \ \alpha = \alpha_o, \tag{3}$$

and the global Nusselt number, defined as

$$Nu = \frac{\alpha_i - \alpha_o}{2\pi} Q, \tag{4}$$

gives the ratio of the total heat transfer to the heat transfer in the absence of convection.

Numerical solution

The above equations were solved using second-order centred finite differences on a 101×151 ($\alpha \times \beta$) regularly spaced grid covering half the annular space since symmetry about the vertical central line was assumed.

The steady-state solutions were obtained by a time marching iterative scheme based on the alternating-direction implicit method (ADI) coupled with cyclic reduction. For each iteration ($n \rightarrow n + 1$), new temperature values (T^{n+1}) were calculated by applying one step of the ADI method to the parabolic equation (1), using the most recently calculated values of the stream function (ψ^n). The latter values were then updated by solving the Poisson equation (2). The finite difference expression for the first ADI half-step, implicit in the α direction, is written as

$$\left(\frac{2h_{i,j}^2}{\Delta t} - L_\alpha \right) T_{i,j}^{n+1/2} = \left(\frac{2h_{i,j}^2}{\Delta t} + L_\beta \right) T_{i,j}^{n}, \tag{5}$$

and the second half-step, implicit in the β direction, is

$$\left(\frac{2h_{i,j}^2}{\Delta t} - L_\beta \right) T_{i,j}^{n+1} = \left(\frac{2h_{i,j}^2}{\Delta t} + L_\alpha \right) T_{i,j}^{n+1/2}, \tag{6}$$

where Δt is the time-step. The finite difference operators L_α and L_β are defined by

$$L_\alpha T_{i,j} = \frac{T_{i-1,j} - 2T_{i,j} + T_{i+1,j}}{(\Delta\alpha)^2} + \frac{\psi^n_{i,j+1} - \psi^n_{i,j-1}}{2\Delta\beta}\frac{T_{i+1,j} - T_{i-1,j}}{2\Delta\alpha}$$

and

$$L_\beta T_{i,j} = \frac{T_{i,j-1} - 2T_{i,j} + T_{i,j+1}}{(\Delta\beta)^2} - \frac{\psi^n_{i+1,j} - \psi^n_{i-1,j}}{2\Delta\alpha}\frac{T_{i,j+1} - T_{i,j-1}}{2\Delta\beta},$$

where $\Delta\alpha$ and $\Delta\beta$ are the grid spacings in the α and β directions, respectively. Subtracting (5) from (6) yields

$$\left(\frac{2h^2_{i,j}}{\Delta t} - L_\beta\right) T^{n+1}_{i,j} = \frac{4h^2_{i,j}}{\Delta t} T^{n+1/2}_{i,j} - \left(\frac{2h^2_{i,j}}{\Delta t} + L_\beta\right) T^n_{i,j}, \tag{7}$$

which is computationally more efficient than solving (6), since it eliminates the need to calculate $(2h^2_{ij}/\Delta t + L_\alpha)T^{n+1/2}_{ij}$. In practice the pair of equations (5,7) are used. The tridiagonal linear systems of equations arising in each half-step were solved using the Thomas algorithm.

The five-point finite difference approximation of the Poisson equation (2) is

$$\frac{\psi_{i-1,j} - 2\psi_{i,j} + \psi_{i+1,j}}{(\Delta\alpha)^2} + \frac{\psi_{i,j-1} - 2\psi_{i,j} + \psi_{i,j+1}}{(\Delta\beta)^2} = \pm a\, h^2_{i,j}\, Ra \times$$

$$\times \left[\sinh\alpha_i \sin\beta_j \frac{T_{i+1,j} - T_{i-1,j}}{2\Delta\alpha} + (1 - \cosh\alpha_i \cos\beta_j)\frac{T_{i,j+1} - T_{i,j-1}}{2\Delta\beta}\right].$$

The resulting linear system was solved by a direct method using an efficient cyclic reduction algorithm[17], implemented in the subroutine GENBUN of the FISHPACK package[18]. The solver has an asymptotic operation count of $O(N_\alpha N_\beta \log_2 N_\alpha)$. The reader is referred to Buzbee *et al.*[19] and Swarztrauber[20] for further details on the topics of cyclic reduction and other related methods.

The extra unknowns corresponding to the fictitious grid lines $(\alpha, -\Delta\beta)$ and $(\alpha, \pi + \Delta\beta)$ were eliminated using the the symmetry condition, i.e. $T(\alpha, -\beta) = T(\alpha, \beta)$ and $\psi(\alpha, -\beta) = -\psi(\alpha, \beta)$, yielding

$$\begin{cases} T_{i,0} = T_{i,2}, \; T_{i,N_\beta+1} = T_{i,N_\beta-1} \\ \psi_{i,0} = -\psi_{i,2}, \; \psi_{i,N_\beta+1} = -\psi_{i,N_\beta-1} \end{cases} \quad \text{for} \quad i = 2, \ldots, N_\alpha - 1.$$

The use of the ψ values at time t_n in the time integration from t_n to t_{n+1}, together with the second-order accuracy of the ADI method, makes the overall time marching procedure only first-order accurate in time. However, this is not a serious drawback because we are mainly interested in the steady-state solutions, and the coupled scheme still retains the strong stability characteristics of the ADI method.

The calculations were assumed to converge when, for every grid point, the dimensionless temperature difference between two consecutive time-steps was

smaller than a tolerance value TOL, set at 10^{-4} as in Barbosa Mota and Saatdjian[7]. In terms of the dimensional temperature, this can be written as

$$\max_{i,j}\left|\frac{\hat{T}_{i,j}^{n+1}-\hat{T}_{i,j}^{n}}{\hat{T}_{i}-\hat{T}_{o}}\right|<\mathrm{TOL},$$

where n and $n+1$ are any two consecutive time-steps.

In order to calculate the total heat flow, the temperature gradient was computed at the grid points belonging to the cylinders' walls, using the following third-order difference schemes:

$$\left(\frac{\partial T}{\partial \alpha}\right)_{\alpha_i,\beta_j}=\frac{-11T_{1,j}+18T_{2,j}-9T_{3,j}+2T_{4,j}}{6\Delta\alpha},$$

$$\left(\frac{\partial T}{\partial \alpha}\right)_{\alpha_o,\beta_j}=\frac{11T_{N_\alpha,j}-18T_{N_\alpha-1,j}+9T_{N_\alpha-2,j}-2T_{N_\alpha-3,j}}{6\Delta\alpha}.$$

The integral in (3) was calculated using the extended Simpson's rule for $\alpha=\alpha_i$ and $\alpha=\alpha_o$, and the final value of Q was taken as the average of the two calculated values.

Results and discussion

In order to ascertain the validity of the code, preliminary runs for $R=2$ and $\varepsilon=0.01$ were made, and the results were compared with the available experimental and numerical data on horizontal, concentric porous annuli. Figure 2 shows the steady-state global Nusselt number as a function of the Rayleigh number for the values of R and ε mentioned above. The numerical results predict that the transition from the bicellular flow regime towards a four-cell flow regime occurs at $Ra=64$, which is in agreement with the experimental value (65 ± 4) obtained by both Caltagirone[1] and Charrier-Mojtabi *et al.*[9] for the concentric case. The Nusselt numbers calculated here differ by less than 1 per cent from those obtained in previous numerical studies that confirmed the bifurcation mentioned above for the concentric geometry[3,6,7]. This gives further confidence in our results.

The two different flow regimes are shown in Figure 3 for $Ra=180$. For a fixed Rayleigh number, the four-cell flow regime has a higher heat transfer rate than does the bicellular one. This is a consequence of a more efficient fluid mixing due to the additional counter-rotating cells. For this radius ratio and for Rayleigh numbers above 115, a third flow pattern containing six cells was obtained numerically by both Rao *et al.*[3] and Charrier-Mojtabi *et al.*[9] using the Galerkin method. The six-cell flow pattern is not included in this work because the heat transfer enhancement with respect to the four-cell flow regime is not high enough to change the conclusions regarding the optimum choice of

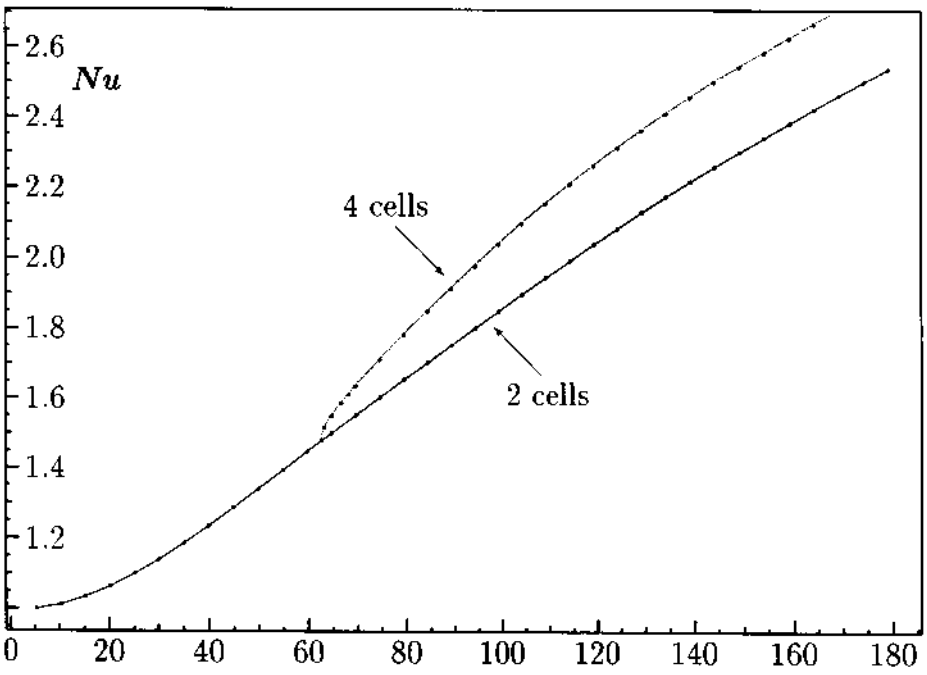

Figure 2. The global Nusselt number (*Nu*) as a function of the Rayleigh number (*Ra*) for $R = 2$ and $\varepsilon = 0.01$. The lower and upper branches of the curve correspond to the bicellular and four-cell flow patterns, respectively

the eccentricity. Moreover, the physical existence of this flow pattern has yet to be proved experimentally.

Figure 2 was constructed by first determining the steady-state solutions for successively larger values of *Ra* using increments of 5. Each successive steady-state calculation was run using the previously converged solution as the initial guess. The initial condition for the first run ($Ra = 5$) was the steady-state solution of the pure conduction regime ($Ra = 0$):

$$\psi = 0, \qquad T = (\alpha - \alpha_o)/(\alpha_i - \alpha_o).$$

At some point in the process the flow pattern changes from two to four cells; this happens despite the fact that no artificial perturbations were introduced in the initial condition. However, this transitional Rayleigh number is not necessarily the minimum one due to a possible hysteresis behaviour of the solution. The true transitional Rayleigh number is obtained by carrying out the calculations in the inverse order, i.e. for decreasing Rayleigh numbers, until the flow transition occurs. The interval containing the flow transition is refined with extra calculations in order to determine the transitional Rayleigh number with an accuracy of ± 0.25. The unfinished part of the lower branch of the Nusselt curve is completed by using a bicellular steady-state solution, obtained previously, as the initial condition for the highest Rayleigh number considered ($Ra = 180$), and then carrying out the calculations for decreasing Rayleigh numbers.

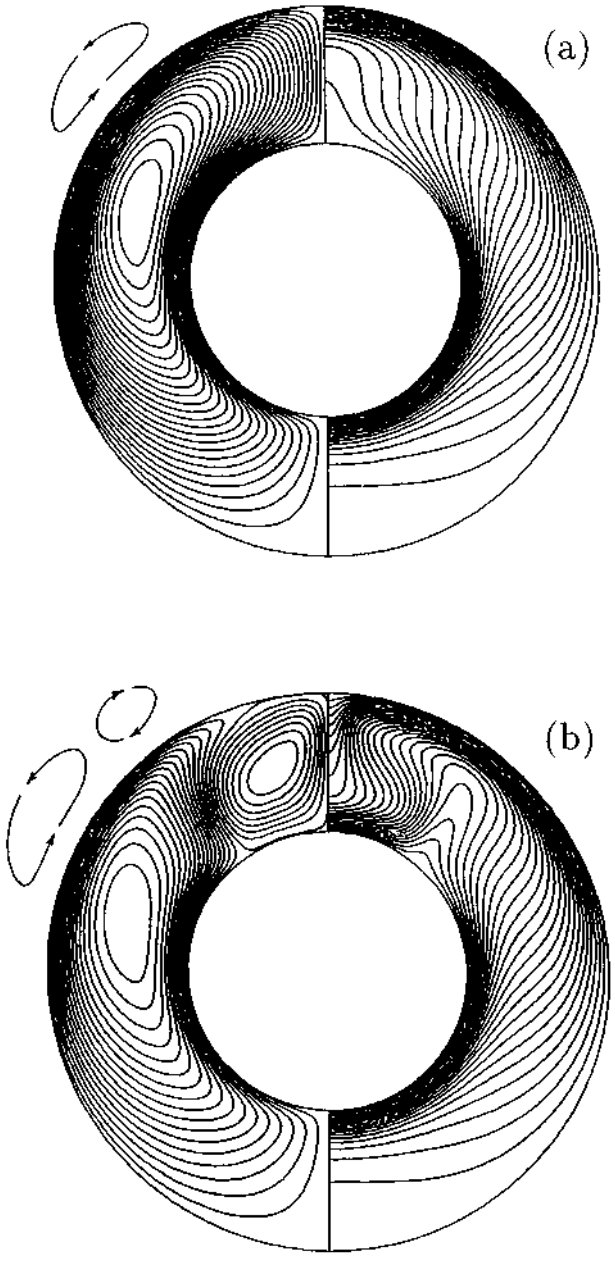

Figure 3.
Streamlines and isotherms for $R = 2$, $\varepsilon = 0.01$, and $Ra = 180$: (a) two-cell flow pattern; (b) four-cell flow pattern. The streamlines and the isotherms occupy the left- and right-hand sides of the annuli, respectively

For $R = 2$, the influence of the eccentricity on the Nusselt number was studied by performing the same procedure for different values of ε. The results are shown in Figure 4. For these runs, the unfinished part of the lower branch of each Nusselt curve was completed by using, as initial conditions, the bicellular

solutions obtained for the same Rayleigh numbers and the previous ε value. For $\varepsilon > 0.5$, we were unable to obtain stable bicellular solutions for Rayleigh numbers above the transition point. For the concentric geometry, Himasekhar and Bau[8] have shown that for $R = 2^{1/2}$ and $R = 2$, two solutions remain stable for some range of Rayleigh numbers, while for $R = 2^{1/4}$ and $R = 2^{1/8}$, the additional solutions appear via a bifurcation process, i.e. one solution branch loses stability while another one gains it. Both observations show a similar trend, this is due to the fact that reducing the radius ratio or increasing the eccentricity has the same impact on the geometry in the top part of the layer where the multicellular structures are concentrated.

As the eccentricity is increased, the transition between the two flow regimes occurs at higher Rayleigh numbers. This is explained by examining the streamlines for $Ra = 100$ and $\varepsilon = 0.1$, 0.4, 0.5 and 0.6, shown in Figure 5. If the Rayleigh number is kept fixed and on decreasing the gap width at the top of the layer, the secondary counter-rotating cell in each half annulus becomes smaller and disappears altogether for $\varepsilon = 0.6$. The elimination of the two secondary counter-rotating cells results in an overall heat transfer reduction. For high values of ε and for $Ra \leq 180$, the gap width in the top part of the layer is very

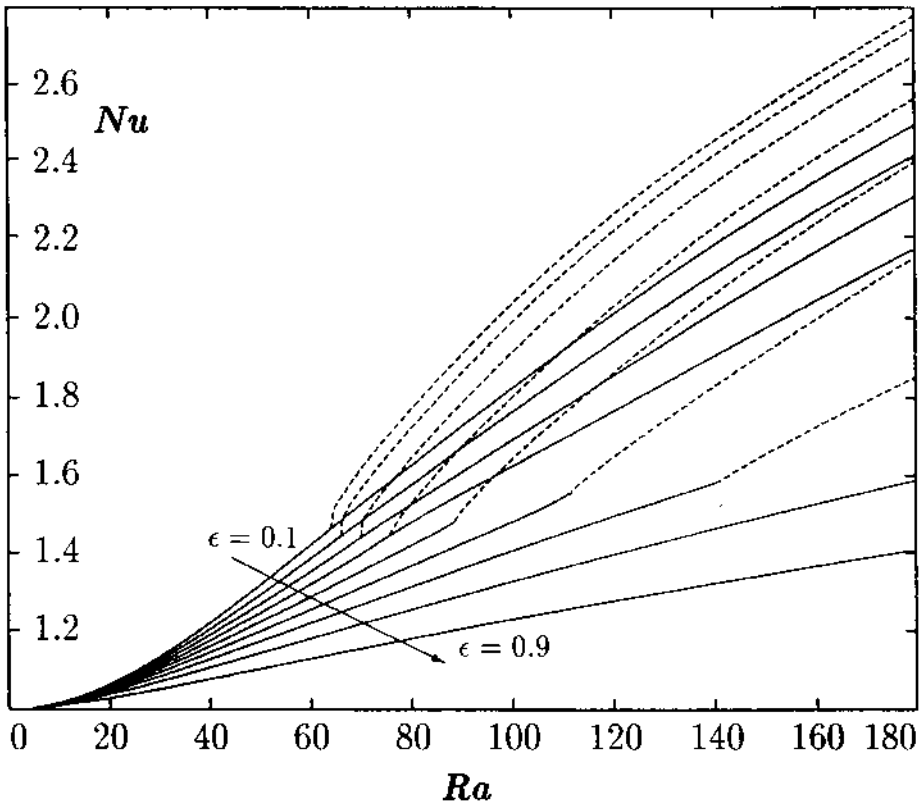

Figure 4. The global Nusselt number (Nu) as a function of the Rayleigh number (Ra) for $R = 2$ and $\varepsilon = 0.1, 0.2, \ldots, 0.9$. The solid and dashed lines correspond to the two- and four-cell flow patterns, respectively

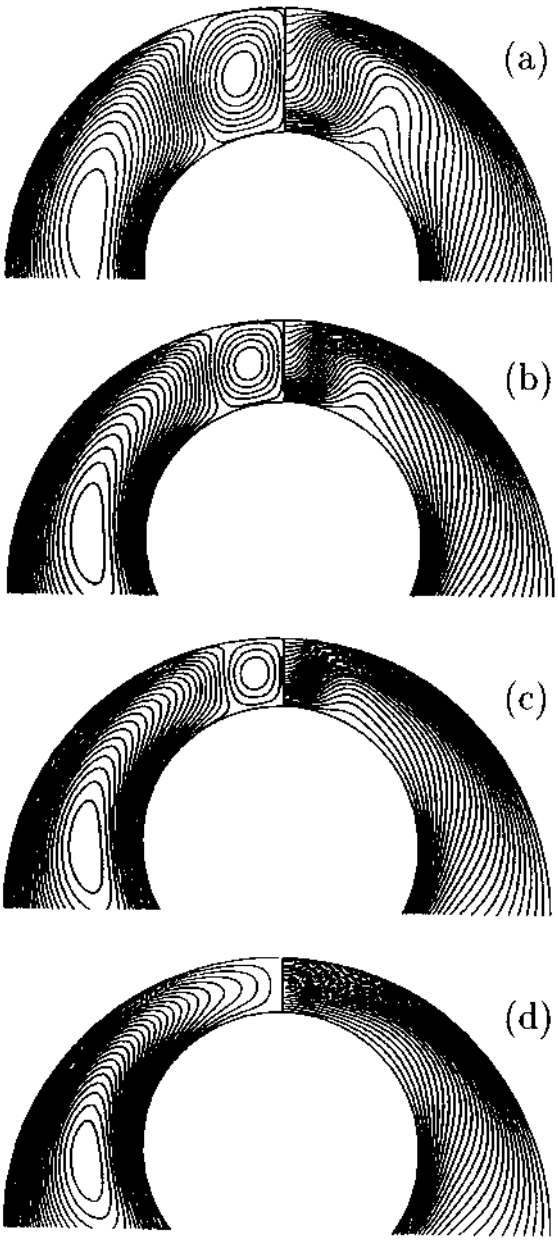

Figure 5.
Streamlines and isotherms in the upper part of the annular layer for $R = 2$, $Ra = 100$, and $\varepsilon = 0.1$(a), 0.4(b), 0.5(c), 0.6(d). The streamlines and the isotherms occupy the left- and right-hand sides of the annuli, respectively

small, thus hindering the appearance of secondary cells. In these geometries, multicellular regimes can occur at very high Rayleigh numbers, the behaviour is similar to that observed in the concentric case with very small radius ratios[6].

In order to search for an optimum configuration leading to a heat transfer reduction, the Nusselt curves presented above were converted to total heat flow curves using equation (4). Figure 6 depicts the overall heat flow rate as a function of the eccentricity for $R = 2$ and $Ra = 110$. As one can see, the lower branch of the heat flow curve, corresponding to the bicellular flow regime, clearly presents a minimum located at $\varepsilon \approx 0.4$. This represents a reduction of 5.7 per cent in the total heat transfer with respect to the same flow regime in a concentric annulus. However, if the four-cell flow pattern prevails in the layer then the minimum of the heat flow curve is located at $\varepsilon = 0.6$. For the radius ratio and Rayleigh number of the figure, this value of ε is the minimum value of the eccentricity for which the two-dimensional bicellular flow is the unique flow pattern. For this value of ε, the heat transfer rate presents a reduction of 11.3 per cent with respect to the four-cell flow pattern in a concentric annulus, and is slightly lower than the one produced by the bicellular flow regime in the concentric case. The results suggest that in a real situation annular insulation with an eccentricity of 0.6 would be more efficient at reducing the heat losses than one having an eccentricity of 0.4, because the former would be better at damping the multicellular structures that are responsible for a steep increase in the heat transfer.

Figure 7 shows, for various Rayleigh numbers, the heat flow rate as a function of the eccentricity. The results presented here for the lower branch of the heat flow curve are in good agreement with those obtained by Bau[11,12]

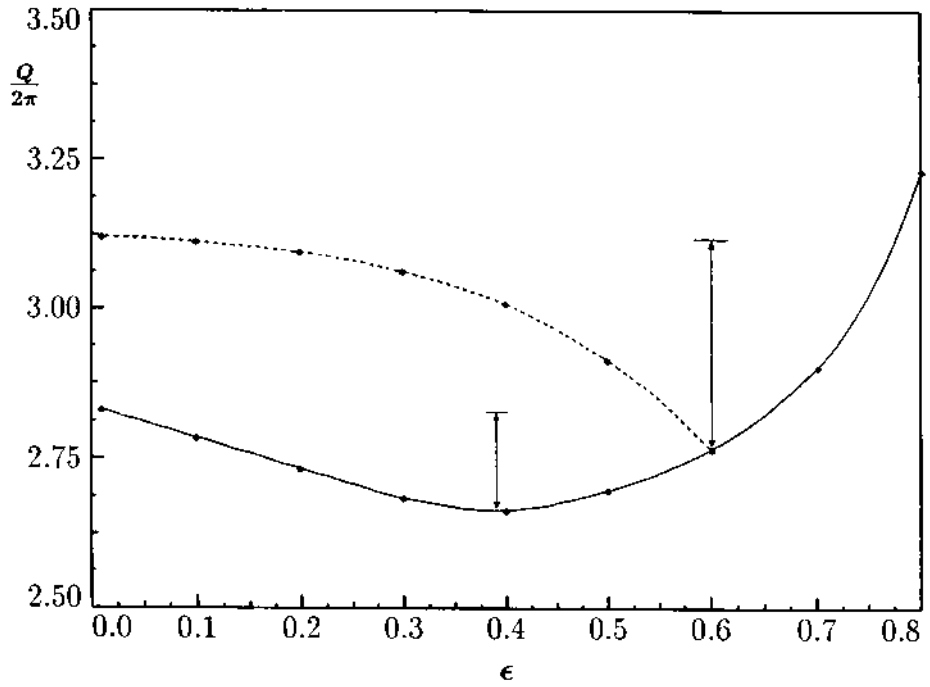

Figure 6. The total heat flow ($Q/2\pi$) as a function of the eccentricity (ε) for $R = 2$ and $Ra = 110$. The solid and dashed lines correspond to the two- and four-cell flow patterns, respectively

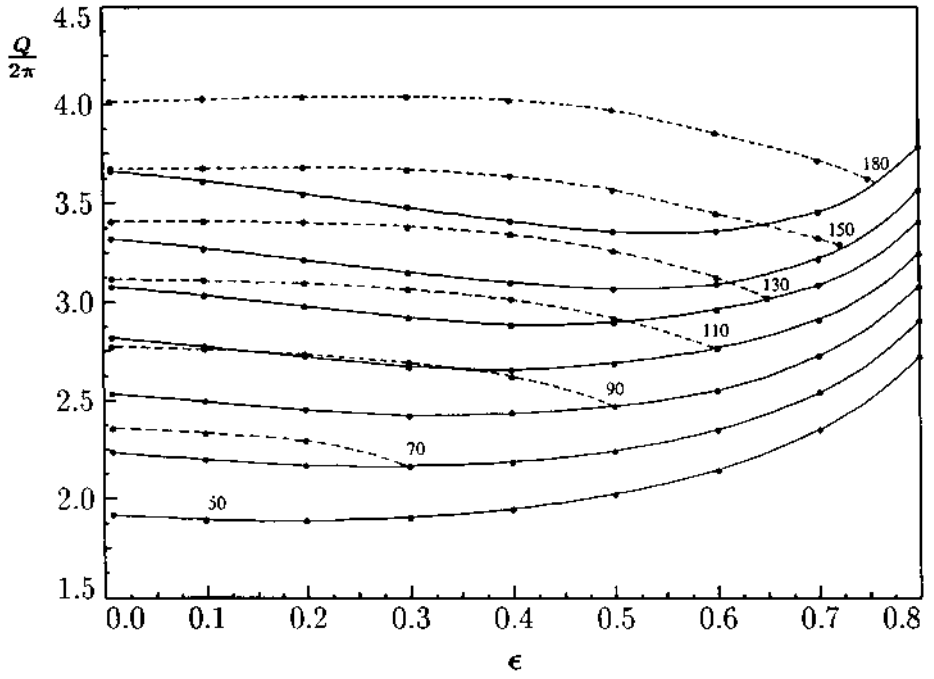

Figure 7.
The total heat flow ($Q/2\pi$) as a function of the eccentricity (ε) for R = 2 and various Rayleigh numbers. The solid and dashed lines correspond to the two- and four-cell flow patterns, respectively

using an extended perturbation expansion and by Bau *et al.*[10] using finite differences. The four-cell flow regime was not observed in those calculations, probably due to a limited radius of convergence of the power series employed in the perturbation expansion and to an insufficient number of grid points (1,320) in the finite-difference mesh. For very small Rayleigh numbers, the heat flow curve is unique and the minimum is located at $\varepsilon = 0$, indicating that for these cases the concentric insulation is the most efficient one. For Rayleigh numbers above the transitional value, the heat flow curve is no longer unique, and the total heat flow can be reduced effectively by an eccentric insulation. The value of the eccentricity that locates the minimum of the lower branch of the heat flow curve increases with the Rayleigh number; the same happens with the minimum value of the eccentricity for which the two-dimensional bicellular flow is the unique flow pattern. For $Ra \leq 180$, the energy savings with respect to the concentric case are of about 10 per cent, if the eccentricity is properly chosen.

Conclusions

An accurate finite-difference code was used to solve the two-dimensional Darcy-Boussinesq equations for an eccentric, horizontal annulus filled with a saturated porous medium. A mesh containing approximately 15×10^3 grid points was used in order to capture the secondary counter-rotating cells in the top of the porous layer. The results obtained for various values of ε ranging

from 0.01 to 0.9, show that reducing the radius ratio or increasing the eccentricity has the same impact on the geometry in the top part of the layer where the convective effects are more pronounced. This strengthens our belief that the study of a single radius ratio, which was set at two for the convenience of comparing with other data, does not remove the generality of the results from the engineering point of view.

For $\varepsilon < 0.5$, the function $Nu(Ra)$ loses uniqueness for Rayleigh numbers above a critical value. Both a bicellular and a tetracellular flow patterns remain stable for the range of Rayleigh numbers studied. For $\varepsilon \geq 0.5$, the transition from one flow regime to the other occurs via a perfect bifurcation, i.e. the flow change occurs with one of the solution branches losing stability. For $Ra \leq 50$, the concentric insulation is the most efficient one for the radius ratio studied. For moderate Rayleigh numbers, raising the inner cylinder centre leads to a reduction of the heat flow, the net gain can be of the order of 10 per cent. The results suggest that in a real situation, insulation is more efficient if ε is set to the maximum value for which the four-cell flow regime is physically realizable rather than to the value that minimizes the heat transfer when the flow pattern is bicellular. Although we studied the case $R = 2$ and moderate Rayleigh numbers, the method employed here can be used to investigate any geometry and Rayleigh number as long as the two-dimensional Darcy-Boussinesq equations remain valid.

References

1. Caltagirone, J.P., "Thermoconvective instabilities in a porous medium bounded by two concentric horizontal cylinders", *Journal of Fluid Mechanics*, Vol. 76, 1976, pp. 337-62.
2. Fukuda, K., Takuta, Y. and Hasegawa, S., *Three-dimensional Natural Convection in a Porous Medium between Concentric Inclined Cylinders*, *ASME*, Orlando, FL, 1981.
3. Rao, Y.F., Fukuda, K. and Hasegawa, S., "Steady and transient analyses of natural convection in a horizontal porous annulus with the Galerkin method", *ASME Journal of Heat Transfer*, Vol. 109, 1987, pp. 919-27.
4. Rao, Y.F., Fukuda, K. and Hasegawa, S., "A numerical study of three-dimensional natural convection in a horizontal porous annulus with Galerkin method", *International Journal of Heat Mass Transfer*, Vol. 31, 1988, pp. 695-707.
5. Barbosa Mota, J.P. and Saatdjian, E., "Natural convection between two horizontal porous cylinders", in *Advanced Computational Methods in Heat Transfer*, Vol. 2, 1992, Elsevier Computational Mechanics Publications, pp. 393-401.
6. Barbosa Mota, J.P. and Saatdjian, E., "Natural convection in a porous, horizontal cylindrical annulus", *ASME Journal of Heat Transfer*, Vol. 116, 1994, pp. 621-6.
7. Barbosa Mota, J.P. and Saatdjian, E., "Natural convection in porous cylindrical annuli", *International Journal of Numerical Methods for Heat & Fluid Flow*, Vol. 5, 1995, pp. 3-12.
8. Himasekhar, K. and Bau, H.H., "Two-dimensional bifurcation phenomena in thermal convection in horizontal, concentric annuli containing saturated porous media", *Journal of Fluid Mechanics*, Vol. 187, 1988, pp. 267-300.
9. Charrier-Mojtabi, M.C., Mojtabi, A., Azaiez, M. and Labrosse, G., "Numerical and experimental study of multicellular free convection flows in an annular porous layer", *International Journal of Heat Mass Transfer*, Vol. 34, 1991, pp. 3061-74.

10. Bau, H.H., McBlane, G. and Saferstein, I., "Numerical simulation of thermal convection in an eccentric annulus containing saturated porous media", *ASME 83-WA/HT-34*, 1983.
11. Bau, H.H., "Low Rayleigh number thermal convection in a saturated porous medium bounded by two horizontal eccentric cylinder", *ASME Journal of Heat Transfer*, Vol. 106, 1984, pp. 166-75.
12. Bau, H.H., "Thermal convection in a horizontal, eccentric annulus containing a saturated porous medium – an extended perturbation expansion", *International Journal of Heat Mass Transfer*, Vol. 27, 1984, pp. 2277-87.
13. Himasekhar, K. and Bau, H.H., "Large Rayleigh number convection in a horizontal, eccentric annulus containing saturated porous media", *International Journal of Heat Mass Transfer*, Vol. 29, 1986, pp. 703-12.
14. Wood, W.W., "The asymptotic expansions at large Rayleigh numbers for the steady motion between non-coaxial rotating cylinders", *Journal of Fluid Mechanics*, Vol. 3, 1957, pp. 159-75.
15. DiPrima, R.C. and Stuart, J.T., "Non-local effects in the stability of flow between eccentric rotating cylinders", *Journal of Fluid Mechanics*, Vol. 54, 1972, pp. 383-415.
16. Wannier, G.H., "A contribution to the hydrodynamics of lubrication", *Quarterly Journal of Applied Mathematics*, Vol. 8, 1950, pp. 1-32.
17. Sweet, R., "A cyclic reduction algorithm for solving block tridiagonal systems of arbitrary dimensions", *SIAM Journal of Numerical Analysis*, Vol. 14, 1977, pp. 706-20.
18. Adams, J., Swarztrauber, P.N. and Sweet, R., *FISHPACK: A Package of Fortran Subprograms for the Solution of Separable Elliptic PDEs*, The National Center for Atmospheric Research, Boulder, CO, 1980.
19. Buzbee, B.L. *et al*., "On direct methods for solving Poisson's equations", *SIAM Journal of Numerical Analysis*, Vol. 7, 1970, pp. 627-56.
20. Swarztrauber, P.N., "The methods of cyclic reduction, Fourier analysis and the FACR algorithm for the discrete solution of Poisson's equation on a rectangle", *SIAM Review*, Vol. 19, 1977, pp. 490-501.